6-1-2001

Characterization of the Kinetic and Mechanistic Differences Between Free-Surface and Bulk Grain Growth in WC-Co Materials

J. M. Olson

Makhlouf M. Makhlouf
Worcester Polytechnic Institute, mmm@wpi.edu

Characterization of the Kinetic and Mechanistic Differences between Free-Surface and Bulk Grain Growth in WC-Co Materials

J.M. OLSON and M.M. MAKHLOUF

The rate of grain growth at different high temperatures in the bulk and at the free surface of a WC-Co substrate was measured. The microstructure, phase evolution, and elemental composition at the free surface were characterized at various stages of the grain-growth process and compared to equivalent characteristics of the bulk. A dramatic difference in the rate of grain growth between the free surface and the bulk of the material was observed. Grains in the free surface grew at a much faster rate than those in the bulk. Since this fast rate of growth was found to coincide with the vaporization of the binder phase from the free surface, it is suggested that this increase in the rate of growth is related to a change in the growth mechanism from an interfacial reaction limited growth in the bulk to a surface diffusion rate limited growth at the free surface. The contact points between grains provide bridges for atomic transport from high free-energy regions (small grains) to low free-energy regions (large grains); hence, the contiguity of the material has a strong influence on the rate of growth.

I. INTRODUCTION

ADVANCES in chemical vapor deposition (CVD) diamond synthesis have led to the development of deposition techniques that are characterized by high deposition rates and large, uniform deposition areas. These techniques have made economical synthesis of diamond films possible and have motivated researchers to explore the use of CVD diamond films for a host of applications. However, several issues that prevent CVD diamond films from achieving their full potential remain unresolved. Paramount among these issues is the poor adhesion of diamond films to their typical WC-Co substrates during direct deposition. The adhesion of CVD diamond films to WC-Co is limited by several factors, including the thermal-expansion mismatch between the film and the WC-Co substrate, the low nucleation density of diamond on WC-Co, and the relatively high solubility of carbon in cobalt. Since traditional CVD diamond synthesis takes place at elevated temperatures (between 700 °C and 900 °C), the thermal-expansion mismatch between the diamond and base material can result in very high residual stresses when the coated material is cooled from the processing temperature to room temperature. These residual compressive stresses can cause spontaneous delamination of the film or may reduce the critical stress for delamination during use. Since CVD diamond growth on WC-Co typically occurs by a Volmer–Weber nucleation and growth mechanism,[1] a low nucleation density can result in the formation of large, internucleic voids at the substrate/diamond interface. These voids can provide crack nucleation sites for interfacial crack propagation and cause delamination of the film. In addition, cobalt is a catalyst for the formation of graphite under typical conditions for CVD of diamond films. Therefore, if cobalt is present at the diamond/WC-Co interface, it can catalyze the formation of a layer of graphite that can obstruct chemical bonding between the film and the substrate. Moreover, cobalt can transform the diamond film that has already formed into graphite. At the elevated temperatures of CVD diamond growth, the transformed graphite is driven into solid solution with cobalt, thus dissolving the diamond film from the interface and decreasing adhesion strength. Therefore, in order to maximize the adhesion strength of diamond coatings to WC-Co substrates, the WC-Co surface must be carefully tailored. This may be accomplished by optimizing three key characteristics of the surface: (1) its chemical composition, (2) its microstructure, and (3) the relative amounts of the phases at the surface. The chemical composition of the surface must be optimized to ensure that deleterious binder/diamond reactions do not occur during deposition and that both a high nucleation density and a high density of direct chemical bonds between the diamond film and the substrate exist. In addition, the microstructure of the WC-Co surface must be optimized in such a way as to minimize crack nucleation sites at the diamond/substrate interface caused by interfacial voids and to provide a toughening crack-deflection mechanism that resists interfacial crack propagation.

Although methods for obtaining such optimum WC-Co substrates have been developed and used (*e.g.*, Reference 2), the fundamental mechanisms that govern the evolution of the desirable surface characteristics are not fully understood. In this publication, a mechanism that explains the evolution of grain structure in the surface of WC-Co substrates is presented. Specifically, the rate of grain growth of the WC phase is characterized at the free surface and compared to that within the bulk of a commercial WC-Co material. The isothermal and temperature-dependent grain-growth-rate constants and activation energies are determined for both cases, and a mechanism that explains the observed microstructure, as well as thermodynamic and kinetic differences in the rate of grain growth between the WC phase at the free surface and within the bulk, is proposed. The

J.M. OLSON, formerly Research Engineer with Saint-Gobain Industrial Ceramics, Northborough, MA, is Staff Process Engineer, Fairchild Semiconductor, South Portland, ME 04106. M.M. MAKHLOUF, Associate Professor of Mechanical Engineering, is with Worcester Polytechnic Institute, Worcester, MA 01609.

Manuscript submitted January 13, 2000.

identification of this grain-growth mechanism should have important ramifications on other areas of study of these materials (particularly, adhesion of coatings to WC-metal carbide-Co substrates) and on the development of methods and grain-growth inhibitors to mitigate excessive grain growth in WC-metal carbide-Co alloys.

II. BACKGROUND

Normal grain growth in WC-Co materials is typically driven by the reduction in surface free energy associated with the interphase boundaries of the system.[3–6] Since tungsten and carbon are mutually soluble in cobalt, small WC particles dissolve during sintering. Growth by solution precipitation of a solid phase in the presence of a liquid can be described mathematically using Eq. [1]:[5]

$$R^n - R_0{}^n = 2Kt \qquad [1]$$

In Eq. [1], R is the mean particle radius after some time (t), R_0 is the initial particle radius, K is the temperature-dependent constant for a given system, and $n = 2$ or 3; $n = 2$ applies when the grain-growth process is limited by the rate at which the atoms or molecules of the solid leave the solid/liquid interface, and $n = 3$ applies when the growth process is limited by the rate of diffusion of atoms or molecules of the solid phase in the liquid. Equation [1] was derived for the simplified case of solid spherical particles in a liquid matrix where the individual particles are not in contact with one another, a case which is clearly not satisfied by typical WC-Co materials. Nevertheless, the technical literature generally reports investigations of grain growth for this class of materials using this general equation. While $n = 3$ has been used occasionally,[7] it is generally accepted that grain growth in WC-Co materials is limited by interfacial reactions and, therefore, is best described using $n = 2$.[8–11]

Diffusion of atoms across the grain boundary is usually considered an activated process and is described by Eq. [2]:

$$K = K_0 e^{-Q/RT} \qquad [2]$$

In Eq. [2], Q is the activation energy for the process. For $n = 2$, Wagner[5] gives

$$K = (64\ \gamma_i\ \Omega^2/81\mathrm{R}T)k_r C_0 \qquad [3]$$

In Eq. [3], γ_i is the solid/liquid interface free energy per unit area, Ω is the molecular volume of the solid, R is the gas constant, T is the absolute temperature, k_r is the rate constant for the reaction causing the transfer of atoms from the solid to the liquid, and C_0 is the solubility of the solid phase in the liquid phase. Using Eq. [2], the grain-growth law may be written as

$$(D^2 - D_0{}^2)/t = K_0 e^{-Q/RT} \qquad [4]$$

From which

$$\ln\left((D^2 - D_0{}^2)/t\right) = \ln K_0 - Q/\mathrm{R}T \qquad [5]$$

Examination of Eq. [5] shows that the quantity $\ln((D^2 - D_0{}^2)/t)$ varies linearly with $1/T$ with a slope of $-(Q/\mathrm{R})$ and a y-intercept that yields the constant K_0.

For interface-controlled Ostwald ripening, the rate of grain growth may be assumed to depend linearly on the driving force, *i.e.*, on the grain-size difference.[5] Eventually, the system reaches a steady state where the normalized grain-size distribution remains invariant. Normally, this grain-size distribution is relatively narrow, with the largest grain being only 2.25 times larger than the average grain.[12,13]

III. MATERIALS AND PROCEDURES

The samples used were WC-Co cutting-tool inserts, with a composition of 94.0 wt pct WC and 6.0 wt pct Co.* The average grain size of the WC phase in the samples was between 1 and 2 μm. In order to investigate the effect of heat treatment on the characteristics of the WC phase, samples were laser scribed with individual identification numbers and weighed.** The samples were then placed on a graphite plate inside an atmosphere furnace, and the temperature within the furnace was increased at a rate of 20 °C/min up to a steady-state temperature of 1550 °C. Specimens were heat treated at this temperature for a variety of soak times ranging from 8 to 95 minutes. A uniform flow of high-purity nitrogen gas at a rate of 100 standard cm^3/min was maintained in the furnace, and the temperature, ramp rate, and gas flow rate were all continuously monitored and controlled throughout the experiments.

In order to investigate the effect of soak temperature on the characteristics of the WC phase, identical experiments to those used in the isothermal experiments were conducted, except that, in this case, the samples were heat treated for 45 minutes at 50 °C intervals between 1350 °C and 1650 °C.

Following each heat-treatment cycle, the final mass of each sample was recorded and the mass loss due to vaporization of the binder phase was calculated from the difference of pre- and postheat-treatment masses. X-ray diffraction (XRD) was used to characterize the composition of the various phases in the samples, and scanning electron microscopy (SEM) and energy-dispersive spectroscopy (EDS) were used to characterize the microstructure and to determine the grain size and composition of the WC phase at the free surface and within the bulk of the WC-Co samples. A field emission scanning electron microscope* was used to examine the microstructural changes in the WC phase at the free surface and within the bulk of the samples. The system was equipped with an energy-dispersive X-ray analyzer that was operated in scan, dot-map, and spot modes in order to identify the composition of particular features of interest. The SEM images were used to characterize the average grain size and morphology of the WC phase at the free surface of each sample. Due to the complexity of the microstructure and difficulties in resolving grain boundaries, computer-aided image analysis to quantify the average size and distribution of the WC grains was not possible; consequently, grain-size determination was performed manually on the SEM images using the method developed by Wasen and Warren.[14] The SEM micrographs of each sample were obtained at various magnifications in order to ensure that measurements of at least 50 grains could be performed for each sample, and all

*Manufactured by Sandvik Coromant, Fair Law, NJ.

**A Mettler model AE50 microbalance was used, Mettler-Toledo, Inc., Columbus, OH.

*TopCon, ABT model 150F was used.

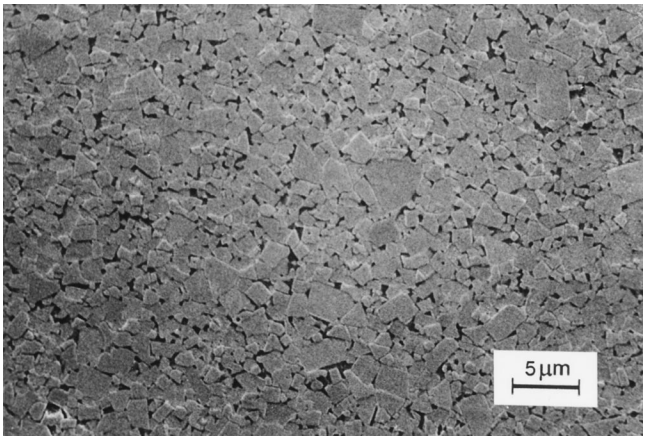

Fig. 1—The surface of a typical WC-Co sample in the as-received condition.

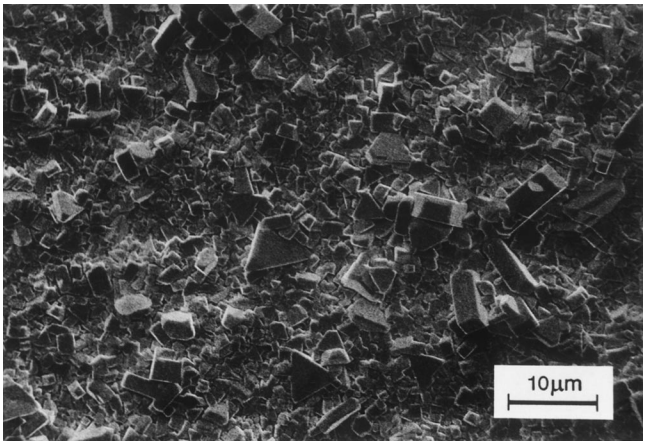

Fig. 2—The surface of WC-Co sample after heat treatment at 1550 °C for 8 min.

efforts were made to ensure that smaller WC grains were accounted for. The maximum chord length of all grains included within the image was measured manually and recorded for the free surface and for the center of the bulk of each sample. EDS was used to examine the free-surface chemical composition and to determine the time-dependent presence and distribution of the binder phase at the free surface.

IV. RESULTS AND DISCUSSION

Figure 1 shows a typical microstructure of the surface of the WC-Co samples in the as-received condition. There are residual grind lines left over from surface grinding, and the ductile binder phase is smeared across the surface. The brittle WC phase is slightly damaged, and fragments of WC grains are imbedded in the smeared grains. Examination of the surface with EDS revealed the presence of W and Co.

A. *Isothermal Heat Treatment*

Figure 2 shows the surface of the samples after heat treatment for 8 minutes at 1550 °C. The binder phase at the free surface has partially vaporized, revealing WC grains that

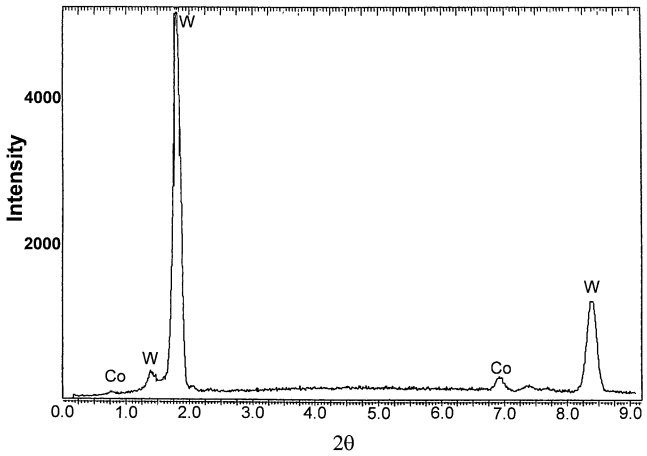

Fig. 3—EDS spectrum of a WC-Co sample after heat treatment at 1550 °C for 8 min.

are nearly equiaxed. EDS analysis of the samples revealed that vaporization of the binder phase is more complete in areas where relatively larger grains are present. The presence of Co at the interstices of the grain boundaries of the relatively smaller grains was detected using EDS in spot and dot-mapping modes. The EDS spectrum, shown in Figure 3, was generated in the scan mode to illustrate the elemental composition of the surface. After longer soak times, the WC particles continue to increase in size as the binder phase at the free surface continues to vaporize. After 20 minutes at 1550 °C, the number of faceted trigonal WC grains increases, as shown in Figure 4(a). While less free-surface Co is detected using scan-mode EDS, spot-mode EDS reveals Co remaining at the interstices of relatively smaller WC grains. No difference was observed between the XRD patterns for the 8- and 20-minute heat treatments. After heat treatment for 38 minutes at 1550 °C, the average particle size of the WC phase at the free surface increases dramatically, as shown in Figure 4(b). Spot-mode EDS analysis of the specimen's surface shows that only a negligible amount of Co is present at the free surface. No change in the XRD pattern between this sample and samples from the 8- and 20-minute heat treatments was evident. After 40 minutes and after 55 minutes at 1550 °C, the WC grains at the surface continue to become more platelike and increase in size, as illustrated in Figure 4(c). No Co is detected at the free surface by scan-mode and by spot-mode EDS, and no change in the XRD pattern is observed between this sample and samples from the 8-, 20-, and 38-minute heat treatments. After heat treatment for periods of $t > 90$ min at 1550 °C, the WC particles at the free surface appear to stratify into thin sheets, as shown in Figure 4(d). At this point, XRD spectra reveal the presence of the η phase.* The EDS analysis of these specimens shows no observable change in free-surface Co from samples heat treated for 55 minutes. After heat treatment at 1650 °C for 45 minutes, the samples lose an average of 4.03 pct of their original weight. At this temperature, identification of individual particles is nearly impossible, and the free-surface morphology corresponds to a well-developed η phase, as shown in Figure 5.

*The η phase is cubic, and its composition has been reported as WC_6Co_3 and as $WC_{12}Co_3$.

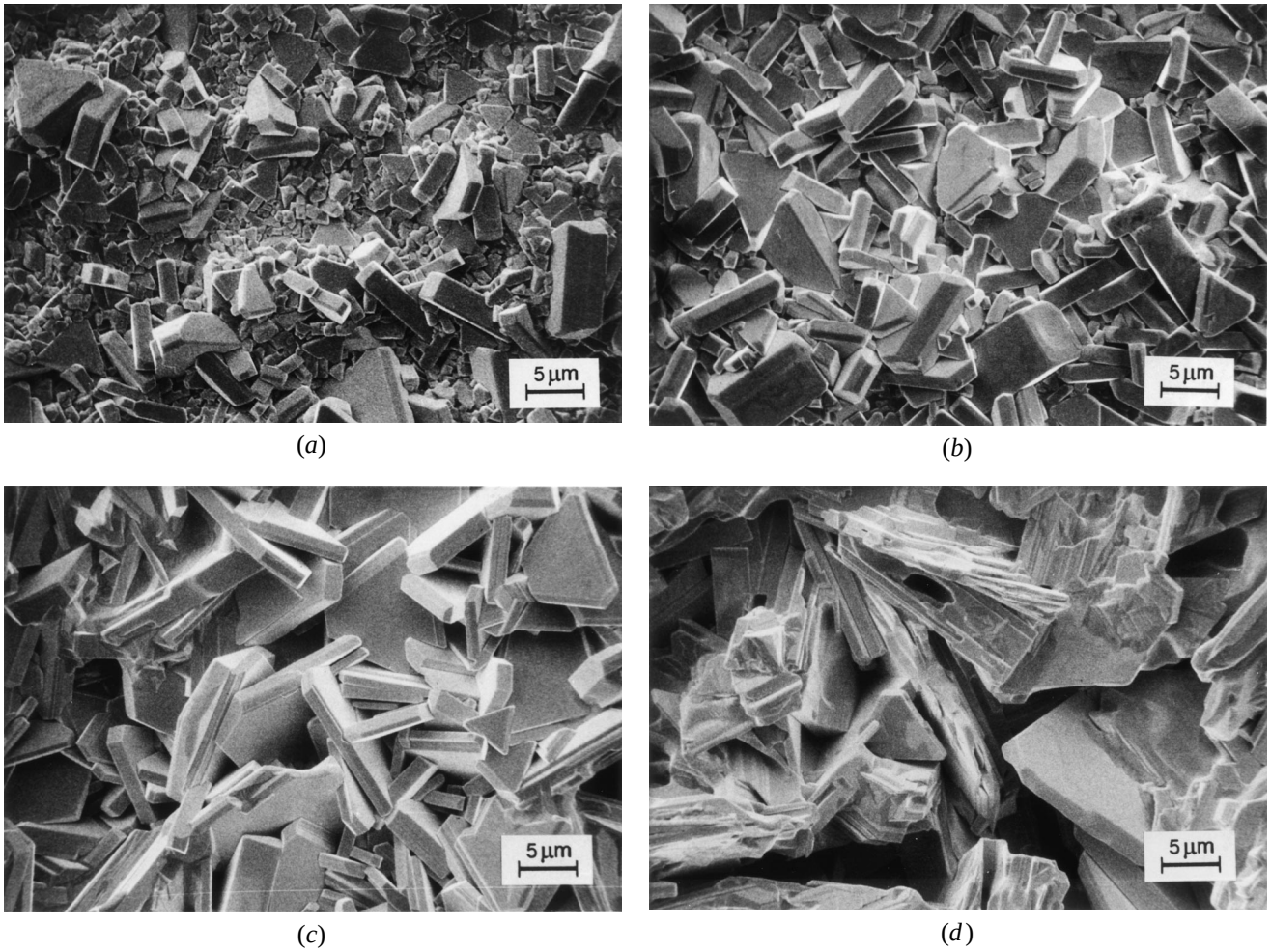

(*a*) (*b*) (*c*) (*d*)

Fig. 4—The surface of a WC-Co sample after heat treatment at 1550 °C for (*a*) 20 min, (*b*) 40 min, (*c*) 55 min, and (*d*) 95 min.

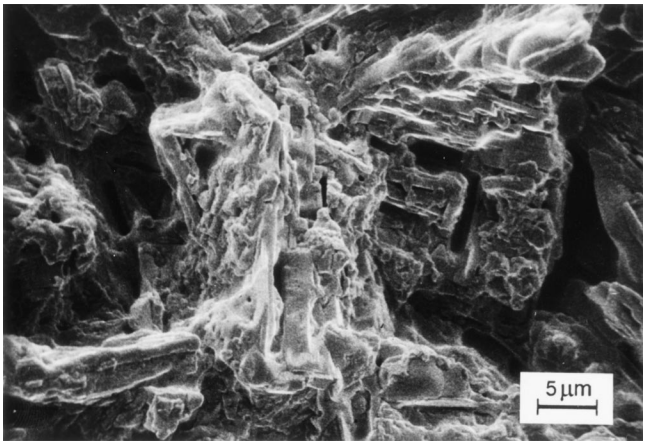

Fig. 5—The surface of a WC-Co sample after heat treatment at 1650 °C for 45 min showing a well-developed η phase.

SEM micrographs of the surface and of polished cross sections from these samples were prepared, and the average particle size of the WC phase at the free surface and within the bulk was determined from these SEM micrographs. Table I summarizes the results of the particle-size analysis.

Rearranging Eq. [2] and using $n = 2$ yields

$$\frac{(D^2 - D_0^2)}{t} = K \qquad [6]$$

Therefore, fitting a linear function to the variation of the difference in the square of the grain size with time for the data in Table I yields the isothermal grain-growth constant (K). The plot, which is presented in Figure 6, shows that the isothermal grain-growth rate in the bulk of the samples (K_{bulk}) is approximately constant throughout the range of heat-treatment times examined. The magnitude of K_{bulk} is calculated to be approximately 3.3×10^{-12} cm^2/s. On the other hand, the isothermal grain-growth rate at the free surface ($K_{surface}$) increases dramatically after 40 minutes of heat treatment. Since the growth rate appears linear within each of the two periods of $t < 40$ min and $t > 40$ min, the data are separated into two sets, and $K_{surface}$ is determined for each set. The magnitude of K at the free surface is approximately equal to that within the bulk, *i.e.*, 3.3×10^{-12} cm^2/s for $t < 40$ min, and is approximately 5.0×10^{-10} cm^2/s for $t > 40$ min.

Considering Eq. [3] and using $K_r = 3 \times 10^{-4}$ cm/s, as suggested by Skolnick,[15] together with $\gamma = 250$ mJ/m^2 and $C_0 = 0.025$ mol/cm^3, as suggested by Warren and Waldren,[8] and $\Omega = 1.26 \times 10^{-5}$ m^3/mol, as suggested by Lee *et al.*,[16] a theoretical value for $K = 2 \times 10^{-12}$ cm^2/s is obtained.

Table I. Particle Size of the WC Phase at the Free Surface and in the Bulk of Samples that were Isothermally Heat Treated at 1550 °C for Various Times

Time (Min.)	Δm_{loss} (Pct)	Number of Grains Measured (Free Surface)	Number of Grains Measured (Bulk)	D_{avg} (Free Surface) (μm)	D_{avg} (Bulk) (μm)
8.8	0.40	303	113	1.2 ± 0.3	1.4 ± 0.3
18.3	0.83	165	192	2.0 ± 0.3	1.3 ± 0.3
18.9	0.86	181	170	2.0 ± 0.3	1.3 ± 0.3
22.3	1.01	160	191	2.0 ± 0.3	1.8 ± 0.3
26.2	1.19	150	192	2.7 ± 0.3	1.9 ± 0.3
26.9	1.22	155	194	2.0 ± 0.3	1.7 ± 0.2
39.7	1.80	135	164	2.6 ± 0.3	2.0 ± 0.3
54.6	2.48	165	101	7.0 ± 0.3	1.8 ± 0.3
55.3	2.51	163	104	6.9 ± 0.3	1.7 ± 0.3
94.1	4.27	196	107	12.3 ± 1.0	1.7 ± 0.3

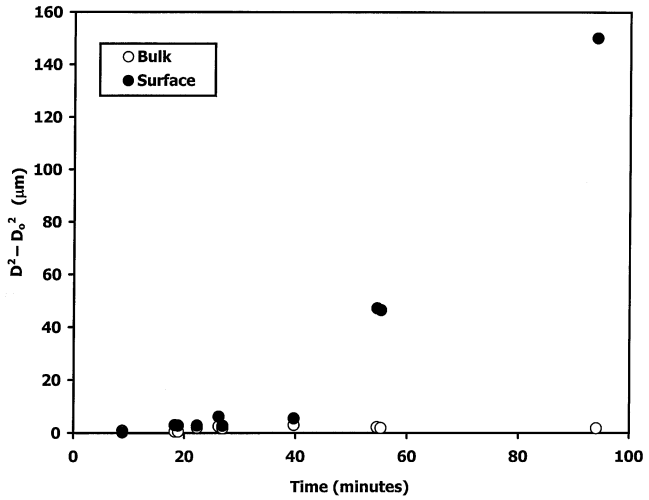

Fig. 6—Graph of ($D^2 - D_0^2$) *vs* time for specimens heat treated at 1550 °C.

This is in excellent agreement with the empirically determined K_{bulk}. Values of K_{bulk} ranging between 0.5×10^{-12} and 10×10^{-12} cm/s have also been reported.[8]

B. *Temperature-Variant Heat Treatment*

Figure 7(a) shows the free surface of samples that were heat treated for 45 minutes at 1350 °C. The samples lost 0.03 pct of their original weight upon heat treatment, and the average grain size of the WC phase at the free surface remained uniform. While some vaporization of the binder phase was observed, a significant amount of Co remained at the free surface of the samples. Figure 7(b) shows the free surface of samples that were heat treated for 45 minutes at 1400 °C. These samples lost 0.10 pct of their original weight upon heat treatment, and the average grain size of the WC phase at the free surface remained uniform and was very similar to samples heat treated at 1350 °C. While vaporization of the binder phase was observed, a significant amount of Co remained at the free surface of the samples, especially at the grain boundaries of the WC grains. Figure 7(c) shows the free surface of samples heat treated for 45 minutes at 1450 °C. These samples lost 0.21 pct of their original weight upon heat treatment, and the average grain size of the WC phase at the free surface remained uniform and was similar to samples heat treated at 1350 °C and 1400 °C. Again, while vaporization of the binder phase was observed, a significant amount of Co remained at the free surface, especially at the grain boundaries of the WC grains. Figure 7(d) shows the free surface of samples that were heat treated for 45 minutes at 1500 °C. These samples lost 0.55 pct of their original weight upon heat treatment. At this temperature, vaporization of the binder phase at the free surface appears greater than at the lower temperatures, yet Co is still present at the grain boundaries of the WC grains, as illustrated by the EDS dot-map image presented in Figure 8. Localized growth of WC grains is apparent in Figure 7(d). After heat treatment for 45 minutes at 1550 °C, the rate of Co vaporization increased significantly, and the samples showed an average weight loss of 2.67 pct. At this temperature, vaporization of the binder phase at the free surface appears to be complete, and Co is not detected at the grain boundaries of the WC grains, as illustrated in the EDS dot-map image presented in Figure 9. The average grain size, which has increased significantly, appears to be uniform, with a dominant trigonal morphology, as illustrated in Figure 10. After heat treatment for 45 minutes at 1600 °C, the samples showed an average weight loss of 3.34 pct. Figure 11 shows that at this temperature, stratification of individual grains into thin parallel plates has occurred, and the average grain size has increased significantly over that of samples heat treated at lower temperatures.

SEM micrographs of the surface and of polished cross sections from the bulk of these samples were prepared, and the average particle size of the WC phase at the free surface and within the bulk was determined from these SEM micrographs. Table II summarizes the results of the particle-size analysis.

The data in Table II show that there is a dramatic increase in grain size for heat treatment temperatures of $T \geq 1500$ °C. This temperature is above the melting point of the binder phase. Since the vapor pressure of metals increases significantly at the onset of melting,[17] it is believed that the increase in the growth rate at $T \geq 1500$ °C corresponds to vaporization of the binder phase from the surface.

Figure 12 shows the variation of ln $(D^2 - D_0^2)/t)$ with $1/T$. Figure 12 shows that, while the activation energy for grain growth within the bulk (Q_{bulk}) is constant over the temperature range studied, the activation energy for grain growth at the free surface ($Q_{surface}$) changes dramatically at $T = 1500$ °C. Treating the data as two separate sets, $Q_{surface}$ is determined for $T < 1500$ °C and for $T \geq 1500$ °C. Table

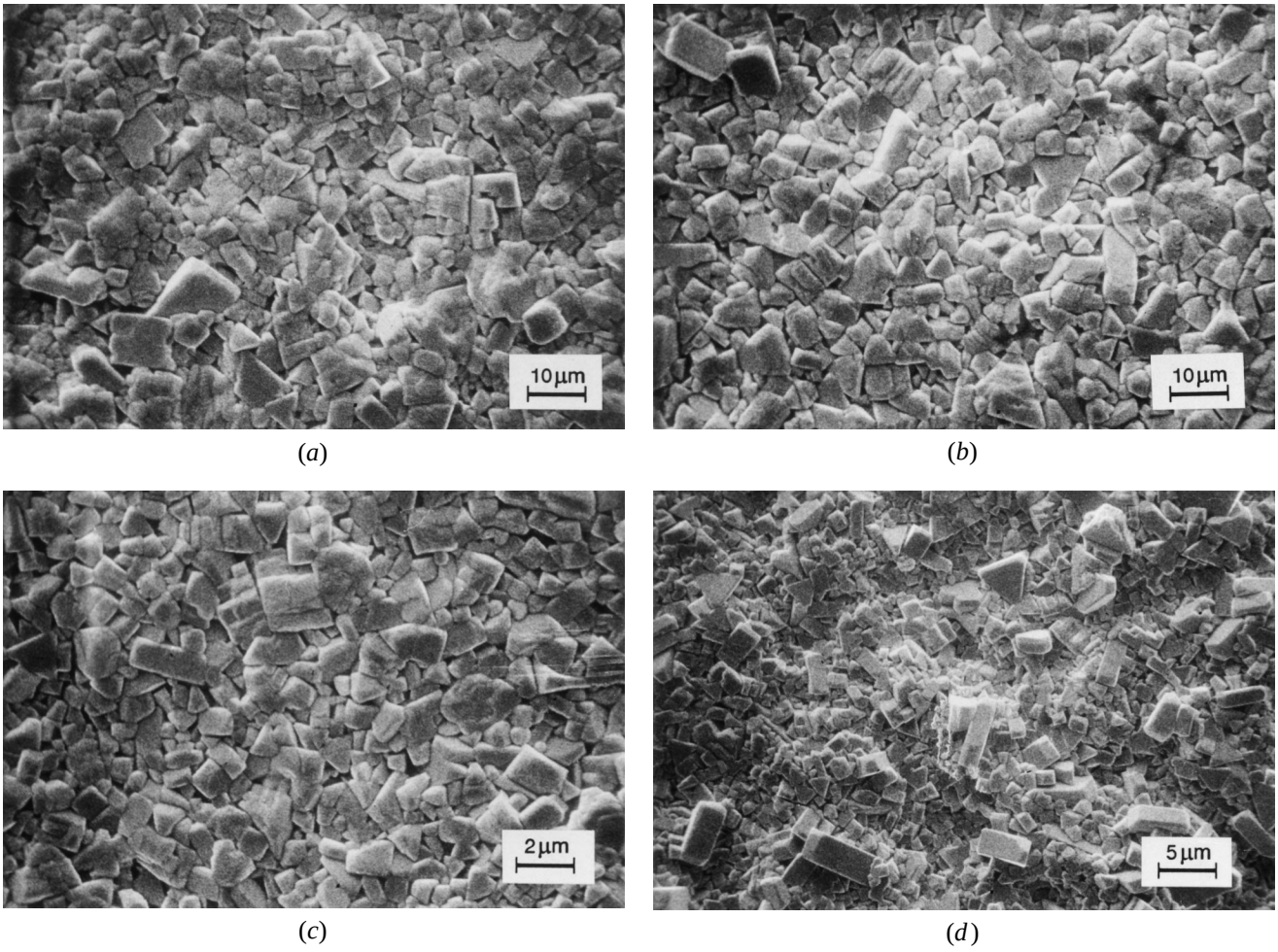

Fig. 7—The surface of a WC-Co sample after heat treatment for 45 min (*a*) at 1350 °C, (*b*) at 1400 °C, (*c*) at 1450 °C, and (*d*) at 1500 °C.

III shows the values of Q determined in this study, together with values reported in the literature.

Examination of Table III shows that the magnitude of the activation energy for bulk grain growth measured in this study is in good agreement with the literature. In addition, the magnitude of the activation energy for free-surface grain growth is equal—within experimental accuracy—to that for bulk grain growth during the initial stages of grain growth. However, the magnitudes of both the activation energy and the grain-growth constant following binder-phase vaporization are anomalous when compared to corresponding parameters for bulk grain growth.

C. *Evolution of the Surface Microstructure*

The SEM micrographs from both the isothermal and temperature-variant experiments show that the WC particles evolve from a mixture of cuboid equiaxed morphology to a platelike trigonal morphology before the onset of the η-phase transformation, as illustrated schematically in Figure 13. Examination of SEM micrographs of specimens heat treated for $t \geq 40$ min at $T > 1500$ °C shows that the dominant morphology is trigonal.

D. *Proposed Mechanism for Free-Surface Grain Growth in WC-Co*

The free energy associated with the interface between a solid phase (S) and a liquid phase (L) in intimate contact is given by[20,21]

$$\gamma_i < \gamma_{SV} - \gamma_{LV} \cos \theta \qquad [7]$$

In Eq. [7], γ_i is the interfacial free energy between the solid and liquid phases, γ_{SV} is the surface free energy of the solid/vapor interface, γ_{LV} is the surface free energy of the liquid/vapor interface, and θ is the contact angle, as illustrated in Figure 14. When the binder phase in WC-Co materials is in the liquid phase, the binder phase completely wets the surface of the WC grains, so that $\theta \approx 0$ and

$$\gamma_i < \gamma_{SV} - \gamma_{LV} \qquad [8]$$

i.e.,

$$\gamma_i < \gamma_{WC} - \gamma_{Co} \qquad [9]$$

Where $\gamma_{WC} = 2.460$ J m^{-2} and $\gamma_{Co} = 0.610$ J m^{-2}.[22] We have shown that the growth rate of WC grains at the surface of WC-Co materials increases dramatically following the vaporization of the binder phase. This can be explained by the fact that in the presence of Co, the interfacial free energy

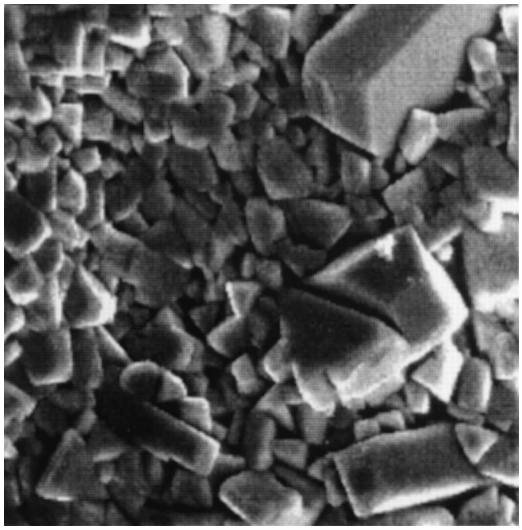

(*a*)

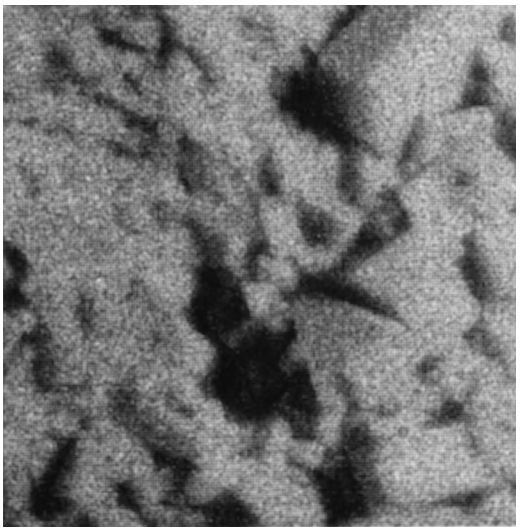

(*b*)

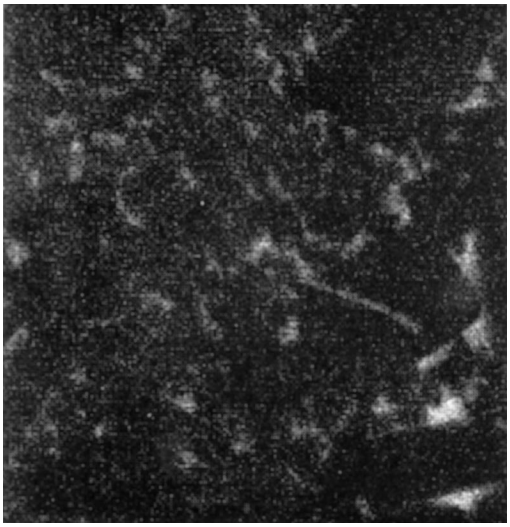

(*c*)

Fig. 8—EDS spectrum of a WC-Co sample after heat treatment at 1500 °C for 45 min: (*a*) image, (*b*) tungsten, and (*c*) cobalt.

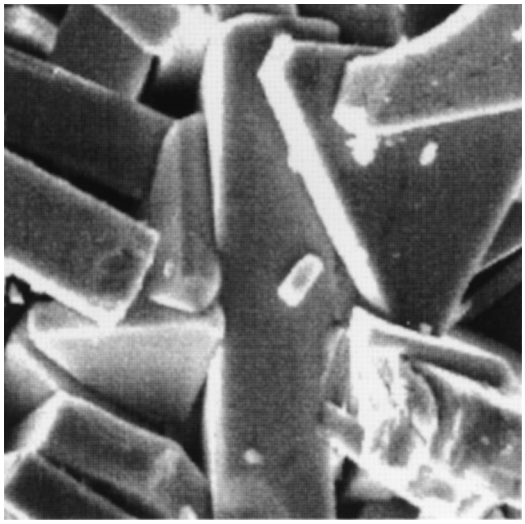

(*a*)

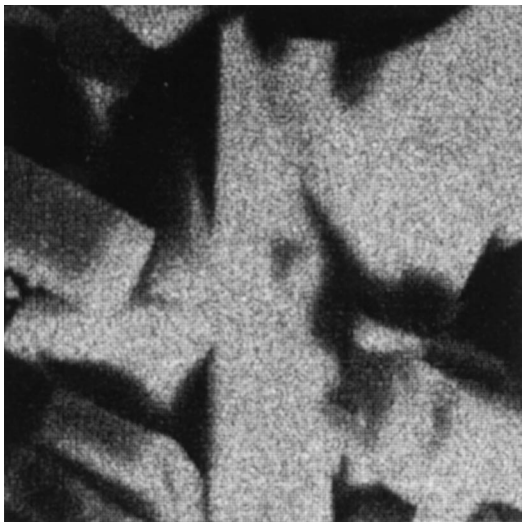

(*b*)

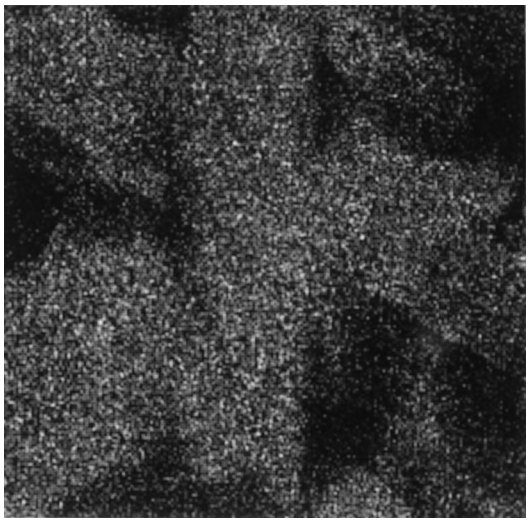

(*c*)

Fig. 9—EDS spectrum of a WC-Co sample after heat treatment at 1550 °C for 45 min: (*a*) image, (*b*) tungsten, and (*c*) cobalt.

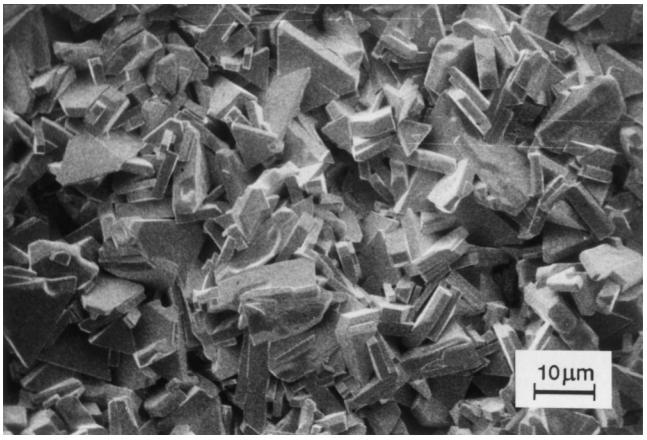

Fig. 10—The surface of a WC-Co sample after heat treatment at 1550 °C for 45 min.

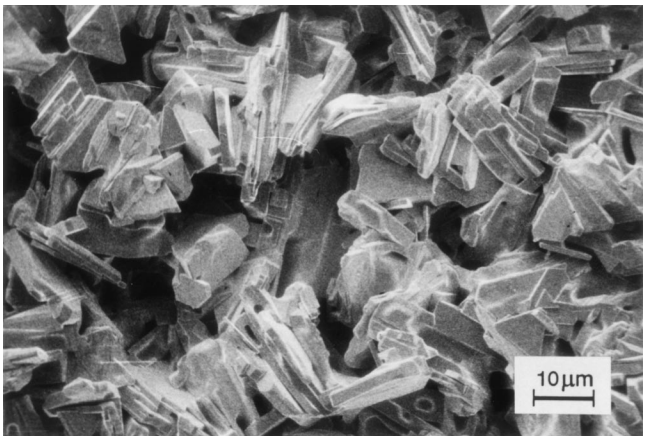

Fig. 11—The surface of a WC-Co sample after heat treatment at 1600 °C for 45 min.

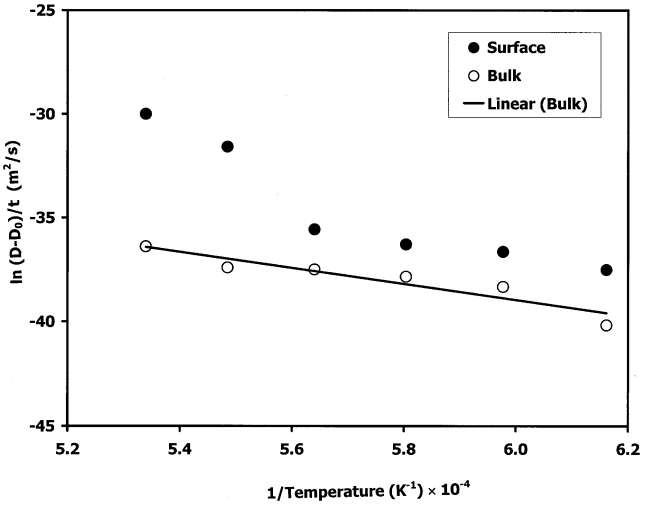

Fig. 12—Graph of ln $\{(D^2 - D_0^2)/t\}$ vs. $1/T$ for specimens heat treated for 45 min. The line represents the best linear fit of the data for bulk grain growth.

γ_i is less than the magnitude of $(\gamma_{WC} - \gamma_{Co})$, but, upon vaporization of the binder phase, γ_i must be less than γ_{WC} only; *i.e.*, vaporization of Co from the surface is attended by an increase of at least 300 pct in surface free energy. We may think of the surface free energy as being proportional to the density of dangling bonds at the surface.[6,23] These dangling bonds act as open sites for atomic "hopping" at the surface.[24] Thus, the increase in surface free energy that results from vaporization of Co from the surface of the WC grains provides for an increase in the mobility of atoms diffusing along the surface, as compared to the mobility of atoms within the bulk of the material.

Further evidence that a surface diffusion mechanism is responsible for the rapid increase in the growth rate is found in the differences in microstructures between the free-surface grains and bulk grains. The SEM micrographs presented in Figures 15 and 16 were taken at the free surface of a sample following vaporization of the free-surface binder phase. At the surface of this sample, growth ledges are observed on the prismatic planes of many of the grains. The microstructure of the ledges suggests that growth occurs by a mechanism in which material diffuses across contact points between particles and along the surface of a growing particle in the form of a growth "front." Thus, it is proposed that the vaporization of the binder phase at the free surface leads to increased atomic mobility and an increase in free energy that reduces the energy barrier for surface diffusion. These factors, coupled with the morphological evidence, suggest that the differences in the growth rate between the bulk and free surface of WC-Co materials is due to a transition in the growth mechanism from interfacial reaction limited growth in the bulk to surface diffusion limited growth at the free surface.

V. SUMMARY

The rate of grain growth at the free surface and in the bulk of a common WC-Co grade substrate in both an isothermal

Table II. Particle Size of the WC Phase at the Free Surface and in the Bulk of Samples That Were Heat Treated for 45 Minutes at Various Temperatures

Temperature (°C)	Δm_{loss} (Pct)	Number of Grains (Free Surface)	Number of Grains (Bulk)	D_{avg} (μm) (Free Surface)	D_{avg} (μm) (Bulk)
1350	0.03	206	153	0.7 ± 0.1	1.1 ± 0.2
1400	0.10	197	117	0.9 ± 0.1	1.1 ± 0.2
1450	0.21	209	191	0.9 ± 0.1	1.2 ± 0.2
1500	0.55	103	160	1.1 ± 0.2	1.3 ± 0.2
1550	2.67	78	111	7.5 ± 0.3	1.2 ± 0.2
1600	3.34	69	134	16.9 ± 0.3	1.4 ± 0.2
1650	4.03	—	152	—	2.0 ± 0.4

Table III. Activation Energy for Grain Growth in WC-Co Materials

Model	Q(kcal/mol)	Reference
WC-Co Liquid Co solution	175	15
WC-10Co Sintering	80	18
WC-10Co Coalescence	142	19
WC-Co	140	11
WC-Co, 10-25 Co Empirical	85	7
WC-6Co Bulk	98	this study
WC-Co Free-surface before complete binder vaporization	108	this study
WC-Co Free-surface following binder vaporization	387	this study

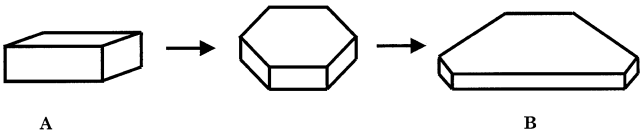

Fig. 13—Schematic illustration of the steps leading to the evolution of the trigonal morphology. The grains begin in an approximately equiaxed structure (A) and develop a truncated trigonal morphology before evolving into the trigonal platelike morphology (B).

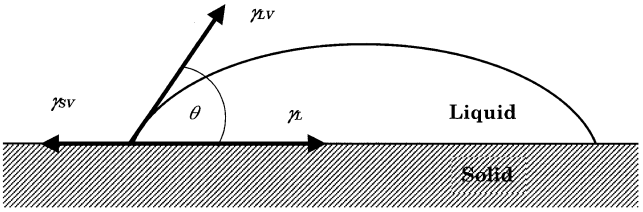

Fig. 14—Schematic representation of a liquid droplet on a solid substrate.

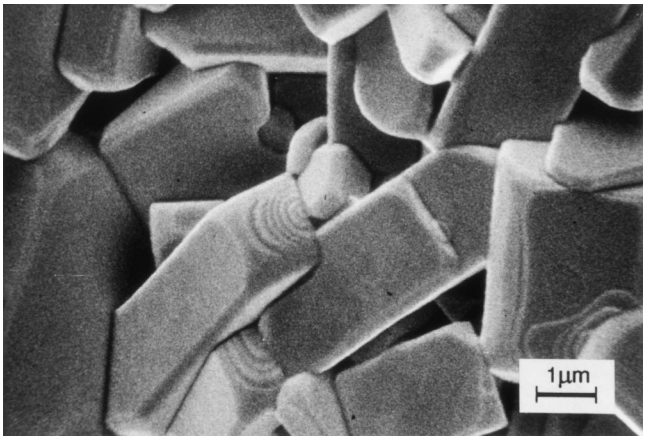

Fig. 15—SEM micrograph showing the formation of growth step fronts on the surface of a WC-Co sample following vaporization of the binder phase from the free surface.

environment and a temperature-variant environment was characterized. The microstructure, phase evolution, and elemental composition at the free surface were characterized at various stages of the grain-growth process and compared to corresponding characteristics of the bulk. It is observed that the rate of grain growth at the surface of these materials

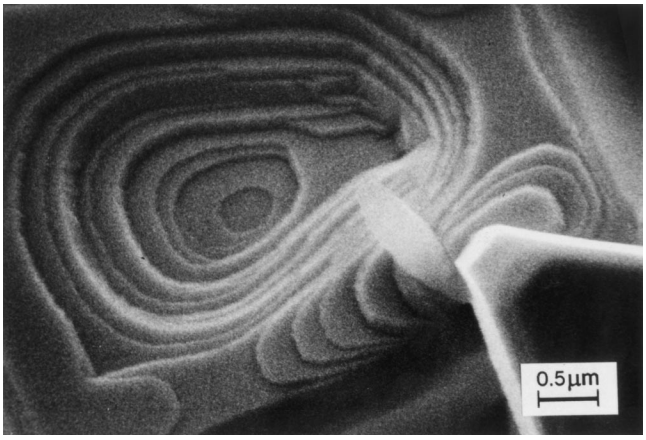

Fig. 16—SEM micrograph showing the formation of growth step fronts on the surface of a WC-Co sample following vaporization of the binder phase from the free surface.

is much faster than in their bulk. It is suggested that this dramatic increase in the rate of growth of the WC phase at the surface coincides with the vaporization of the binder phase from the surface. Growth of the WC grains in the bulk of WC-Co materials has been studied extensively, and it is generally accepted that grain growth in these materials is limited by interfacial reactions. We propose that the fast rate of grain growth at the free surface is due to a change in the grain-growth mechanism from interfacial reaction limited growth in the bulk to a surface diffusion rate limited growth at the free surface.

The identification of this grain-growth mechanism should have very important ramifications on other areas of study of these materials (particularly, adhesion of coatings, *e.g.* diamond films, to WC-metal carbide-Co substrates) and on the development of methods and grain-growth inhibitors to mitigate excessive grain growth in WC-metal carbide-Co alloys.

REFERENCES

1. J.M. Olson: *Proc. Ultrahard Materials Conf.*, Hamilton, ON, 1998, pp. 507-33.
2. J.M. Pineo: European Patent Application 93,308,250.5, 1993.
3. P. Schwarzkopf and R. Kleffer: *Cemented Carbides*, Macmillan Company, New York, NY, 1960, pp. 55-101.
4. H.E. Exner: *Int. Met. Rev.*, 1979, vol. 4, pp. 149-55.
5. C. Wagner: *Z. Elektrochem.*, 1961, vol. 65, pp. 581-91.
6. D.A. Porter and K.E. Easterling: *Phase Transformations in Metals and Alloys*, Chapman & Hall, New York, NY, 1992, pp. 130-71.
7. J.L. Chermant, M. Coster, A. Deschanvres, and A. Iost: *J. Less-Common Met.*, 1977, vol. 52, pp. 177-96.
8. R. Warren and M.B. Waldron: *Powder Met.*, 1972, vol. 15, pp. 180-201.
9. R. Warren: *J. Mater. Sci.*, 1968, vol. 3 (5), pp. 471-85.
10. R. Warren: *J. Mater. Sci.*, 1972, vol. 7 (12), pp. 1434-42.
11. M. Coster and A. Deschanvres: *Comp. Rend.*, 1969, vol. 296, pp. 291-96.
12. C.V. Thompson, H.J. Frost, and F. Spaepen: *Acta Metall.*, 1987, vol. 35, pp. 887-91.
13. Y.J. Park, N.M. Hwang, and D.Y. Yoon: *Metall. Mater. Trans. A*, 1996, vol. 27A, pp. 2809-19.
14. J. Wasen and R. Warren: *J. Inst. Met.*, 1989, pp. 222-26.
15. L. Skolnick: *Kinetics of High Temperature Processes*, MIT, Cambridge, MA, and Wiley, New York, NY, 1959, pp. 92-99.

16 I.C. Lee, H. Hondo, and T. Sakuma: *Scripta Metall. Mater.*, 1993, vol. 28, pp. 97-102.
17. D.R. Gaskell: *Introduction to Thermodynamics of Materials*, 3rd ed., Taylor and Francis, New York, NY, 1995, p. 94.
18. H.E. Exner and H. Fischmeister: *Z. Metallkd.*, 1966, vol. 57, pp. 187-92.
19. H.E. Exner and H. Fischmeister: *Arch Eisenhuttenwes.*, 1966, vol. 37 (5), pp. 417-21.
20. R.H. Doremus: *Rates of Phase Transformations*, Academic Press, New York, NY, 1985.
21. K. Reichelt: *Vacuum*, 1988, vol. 38, pp. 1083-99.
22. R. Warren: *J. Mater. Sci.*, 1980, vol. 15 (10), pp. 2489-96.
23. R.E. Reed-Hill and R. Abbaschian: *Physical Metallurgy Principles*, 3rd ed., PWS Publishing Company, Boston, MA, 1994, pp. 390-94.
24. P.G. Shewmon: *Transformations In Metals*, McGraw-Hill, New York, NY, 1969.